Ae-Based Failure Warning Mechanism During Cemented Paste Backfilling: Experimental Investigation

Chunde Ma[1,2], *Zihe* Wang[1*], *Jiaqing* Xu[1], *Guanshuang* Tan[1], and *Zhihai* Lv[1]

[1]School of Resources and Safety Engineering, Central South University, Changsha 410083, Hunan, China
[2]Center for Advanced Studies, Central South University, Changsha 410083, Hunan, China

Abstract. To research the AE warning mechanism of cemented paste backfilling (CPB), the uniaxial compression test with AE monitoring was carried out on CPB. The effects of different moisture content, cement proportion, and loading rate on AE characteristics of CPB were analyzed. And a damage model based on AE is established. The results show that the increase of water content, gypsum content, and loading rate can enhance the ductility of CPB and lengthen the AE warning area. However, the increase of moisture content will lead to the delay of AE signal peak, which is bad for the early warning. With the increase of loading rate, the failure mode of specimens gradually changes from splitting failure to shear failure. The cracks produced under different failure modes can correspond to the peaks of AE signals. The damage model based on AE shows that the damage process of CPB samples can be divided into three stages, linear-exponential-linear. The experimental results can further research the optimal conditions for ae monitoring of backfill, and provide a theoretical basis for ae monitoring and warning of backfill.

1 Introduction

In China, a large amount of waste rock generated during underground mining accumulates on the surface, which not only occupies land space but also releases harmful elements into the air and water [1]. Filling mining technology is a burgeoning mining technology which uses solid offal such as tailings, construction waste, and abandoned rocks to carry out crushing, screen grading, and then cement and fill mined-out areas [2-4]. It can be used to reduce ore dilution and decrease mining cycles to improve production efficiency [5-6], which brings great benefits to the economy, safety, and environmental protection. In the last few decades, different filling mining techniques had been developed and applied to mine goaf management [7-8]. However, it was found in the engineering practice that the filling mining technology mentioned above has some disadvantages, such as high cost and insufficient utilization of the wastes in the mining process. As a consequence, cementing paste filling has been widely used because of its ability to reduce the cost of waste rock storage and treatment and its environmentally friendly feature [9-10].

As a porous medium consisting mainly of cementing materials, waste rock aggregate, and pores [11], the AE characteristic of CPB is closely related to the choice and the ratio of cementing material, and the aggregate particle size grading, etc. [12-14]. Many types of researches indicated that the loading rate has a significant effect on the properties of materials. Different materials such as rock, concrete, and backfill exhibit different behaviors under different loading rates [15-17].

AE monitoring technology, as one of the important development directions of safety detection and non-contact prediction methods, can detect individual fracture events and provide a basis for the mechanical property analysis of solid materials [18-20]. Many scholars have applied AE technology to study the mechanical properties of solid materials [21-22]. Establishing reasonable failure criteria and using AE signal characteristics as the failure criterion of materials in nondestructive testing is of great importance for the research of the AE characteristics of CPB samples. However, the relationship between the AE characteristics and failure modes of CPB samples and the relationship between AE signals and crack failure surface have been barely researched by scholars.

In this paper, a uniaxial compression test on cemented red sandstone was carried out. Combined with AE detection data, the effects of different moisture content, loading rates, and the ratio of cementing materials on AE characteristic of CPB were discussed. The failure modes of CPB samples under different loading rates and the corresponding relationship between the AE ringing counts and the crack failure surface was revealed. The experimental results have important guiding significance for monitoring AE signals of CPB failure signs and analyzing failure mechanism of CPB in the process of filling mining.

* Corresponding author: csuwangzihe@163.com

2 Materials and Experimental Equipment

2.1 Experimental Materials

2.1.1 The aggregate of CPB samples

As a kind of common solid waste material produced by coal mining, red sandstone can be used as the aggregate of CPB. In this experiment, red sandstone with a natural density of 2.48g/cm^3 and an average strength of 45MPa was used as the material for CPB sample preparation. First, complete red sandstone blocks were crushed into small pieces, followed by further mechanical crushing of the larger ones. Then the grading screen was used to classify the particles, and the gravel particles with a diameter range of 0~2mm, 2~5mm, 5~8mm, 8~10mm, and 10~12mm were uniformly selected as the test samples. According to Talbot Index theory:

$$\frac{M_i}{M} = \left(\frac{d_i}{d_m}\right)^n \quad (1)$$

where n is the Talbot index, Mi is the mass of aggregate whose diameter is less than d_i, and M is the total mass of aggregate. D_m is the maximum diameter of red sandstone material particles, which is 12mm in this experiment. In this paper, a gradation scheme with a Talbot index of 0.5 was used for sample preparation. According to Formula 1, the mass and percentage of each particle size are shown in Table 1.

Table 1. The particle size distribution of the sample

Weight of each particle size (g)				
0~2mm	2~5mm	5~8mm	8~10mm	10~12mm
114.24	66.36	47.88	27.16	24.36

As one of the important factors studied in this paper, cementing material has a great influence on the stress-strain properties and AE characteristics of the CPB sample. In the preparation of the cementing sample, cement and gypsum are often mixed in different proportions as the cementing material of the sample In this paper, 42.5 grade Portland cement and hemihydrate gypsum are used as cementing materials.

2.1.2 Preparation of Specimens

In this paper, the total mass of the cementing materials was set as 100g, and CPB samples were prepared with three ratios of cement to gypsum: 3:1,1:0 and 1:1. Homogeneous slurry consisting of water and cementing materials was adequately mixed and stirred with crushing red sandstone particles. Poured the mixture into a cylindrical mold with a diameter of 50mm and a height of 100mm, and vibrated the bubbles out of the slurry. After initial solidification, the samples were removed from the mold and cured for 28 days in a constant temperature curing box. The two ends were smoothed out after being removed from the curing box, and the test samples were obtained.

As for the samples with different moisture content, the DHG-9035A drying oven was used to dry the samples with a cement/gypsum ratio of 3:1 at 105°C for 24 hours to get the drying samples. After taking out from the drying box, the samples were carried out sealing preservation immediately to ensure the moisture content as the lowest state. The saturated samples were obtained after 24 hours soaking. The moisture content in dry state, natural state and saturated state were measured as 0%, 3.01% and 10.20% respectively. Some samples are shown in Fig. 1.

Fig. 1. CPB samples

2.2 Experimental Equipment

WHY-200/10 microcomputer-controlled automatic experimental machine as shown in Fig.2(a) was used for uniaxial compression test on CPB, whose load accuracy can be controlled within 1%, displacement accuracy can be controlled within 0.5%, and the maximum load range is 300kN.

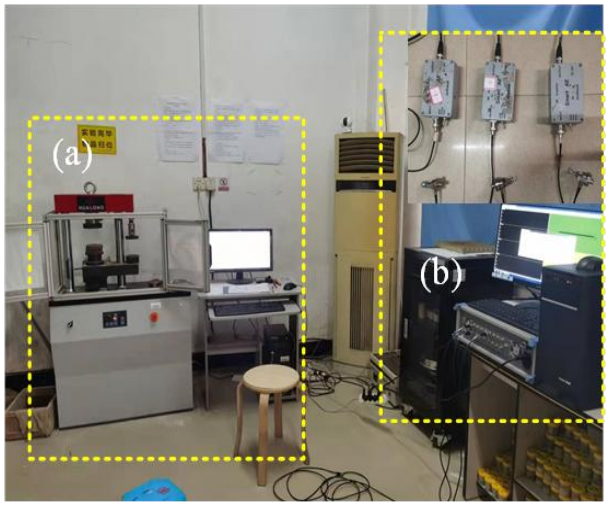

Fig. 2. The loading and AE monitoring integrated acquisition system, (a) WHY-200/10 microcomputer-controlled automatic experimental machine (b) AE monitoring system

The AE monitoring system is shown in Fig.2(b). Set the sampling frequency as 2.5MHz and threshold value as 40dB.The AE sensors were attached equally spaced to the sample. Vaseline was applied between the probe and the sample as a coupling agent to eliminate the influence of head load on AE signals. AE signals were transmitted into the AE acquisition system through the preamplifier, and AE data is formed after noise reduction and screening by the instrument.

2.3 Experimental Methods

CPB test schemes with different cementing material ratios, water content and loading rate were set to study the effects of cementing materials, moisture content and loading rate on the mechanical properties and AE characteristics of CPB samples. The specific parameters of the test scheme are presented in Table 2.

Table 2. Experimental scheme of uniaxial compression

Sample	Mass of cementing material (g)		Loading rate (N/s)	Moisture content (%)
	Cement	Gypsum		
CPB-1				0
CPB-2	75	25	150	3.01
CPB-3				10.20
CPB-4	100	0		
CPB-5	75	25	150	3.01
CPB-6	50	50		
CPB-7			100	
CPB-8	75	25	150	3.01
CPB-9			200	

Certain discrete factors in the mechanical properties of CPB have resulted in the manufacturing operation. To ensure the universality of the test results, three groups of repeated tests were carried out for each sample, and the mechanical parameters were averaged.

3 Results and discussion

3.1 AE characteristic of CPB

3.1.1 AE ringing count characteristics of CPB

It is generally accepted that parameters such as AE ringing count are generated by crack propagation and rock failure. The information on crack propagation in the process of specimen compression can be obtained by AE monitoring. However, there are some problems in the process of tests, such as coupling of sensor and sample, a slight difference of frequency response of the different sensor, and signal attenuation caused by different propagation distance. By comparing the signals received by the sensors with equidistant Settings, AE ringing counts were collected and obtained. After calibration, the time-load-AE ringing count diagrams are shown in Fig.3-5. The results show that during the loading process, the AE ringing count will go through three stages:

(I) Quiet period. At the initial loading stage, tiny cracks and elastic deformation appeared in the sample. AE ringing count is rarely generated, which is in the quiet period of acoustic emission.

(II) Rapid development stage，after the elastic stage, plastic deformation occurs on the samples, cracks generate and expand rapidly until failure. At this time, AE signals appear frequently, the ringing count increases sharply, and the peak value of the AE ringing count appears.

(III) Stable period, in the post-peak phase, the AE ringing count less than the peak value is continuously generated.

3.1.2 Effect of moisture content on AE characteristic

As can be seen from Fig.3, with the increase of water content, the level of AE ring-counts decreases rapidly, but the time range of AE ring-counts increases greatly.

The AE ringing counts generated at yield phase of samples in dry condition were mostly above 500, while the average number of samples in natural condition was around 80 and of samples in saturation condition was between 0 and 50. This was mainly due to the fact that the internal cementation structure of the specimen was damaged after being immersed in water. The sample was softened by water and showed a creeping tendency, and the severity of the internal damage has lessened.

The relative warning area of the sample, which is the ratio between the rapid development period and the whole loading process, obviously increased. In the dry state, no obvious AE ringing counts appear until about 110s, while in the natural state and saturated state samples, obvious AE ringing counts began to appear around the 70s and 20s.

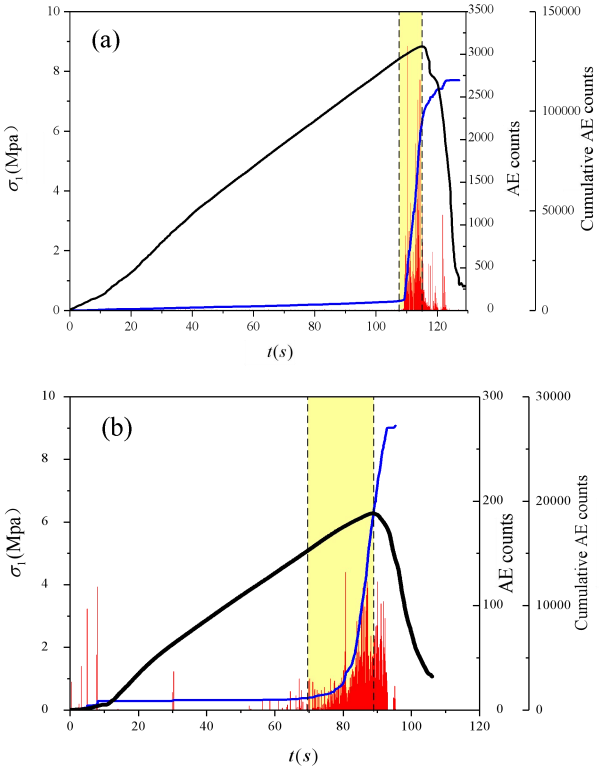

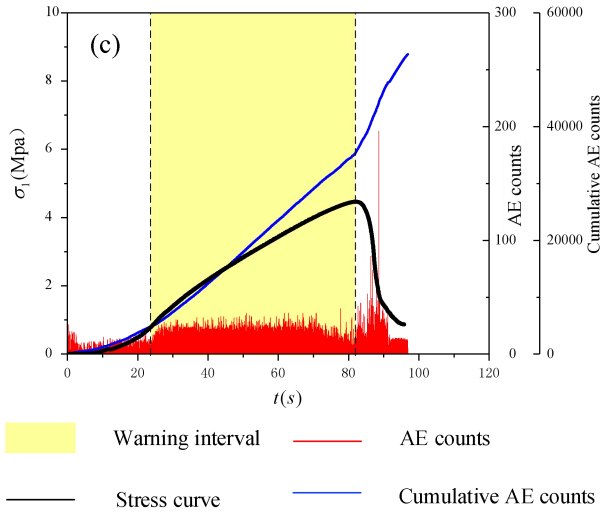

Fig. 3. Evolution of accumulative count of CPB samples with different moisture contents: (a)dry state (b) natural state (c) saturated state

From the time of the AE signal distribution, samples in dry condition had been in a long AE quiet period since the elastic stage. The cracks expanded rapidly at the approach of failure. At yield phase, high-level AE signals suddenly appeared, followed by a peak of the ringing count. The distribution of AE ringing counts was concentrated, and the sample had a tendency of sudden failure. The AE signals of samples in the natural state were more concentrated in the late elastic stage and in yield phase. There were only a few AE signals generated by fracture compaction in the compaction stage, and the maximum value of the AE ringing count appeared near the peak. In saturated samples, new micro-cracks were always generated and expanded after the crack compaction process, and AE signals were ubiquitous in the whole loading process. The maximum value of the AE ringing count appeared after the peak, and there were several similar peaks of the AE ringing count near the maximum point. No sudden increase in AE ringing counts occurred, and the slope of the cumulative ringing count curve had little change.

According to the above, moisture content has a great influence on the type of rock damage. With the increase of moisture content, the CPB specimen experienced significant softening and strength reduction, and the failure type changed from brittle failure to ductile failure. The ability of samples to absorb elastic energy is weakened, releasing energy gradually. Meanwhile, with the increase of moisture content, the peak value of AE ringing counts lags obviously, which greatly weakens the predictive effect of acoustic signals on backfill failure.

3.1.3 Effect of cementing material on AE characteristic

The AE characteristics of CPB samples with different ratios of cementing materials can be seen in Fig.4. With the increase of the proportion of gypsum, the AE ring-counts produced by the development of cracks appeared earlier, and the cumulative AE ring-counts increased more slowly before the peak, the relative warning area becomes significantly longer.

For samples made entirely of cement, the AE ring count became higher and more intensive around the 270s, and the sample reached the peak strength after about 10s. For the sample cement and gypsum ratio of 1:1, the AE ringing counts started to increase significantly at about 72s, and the sample reached the peak strength after about 15s. However, for the sample with cement and gypsum ratio of 1:3, the AE ringing counts began to increase at about 48s, and the sample reached the peak strength after about 18s.

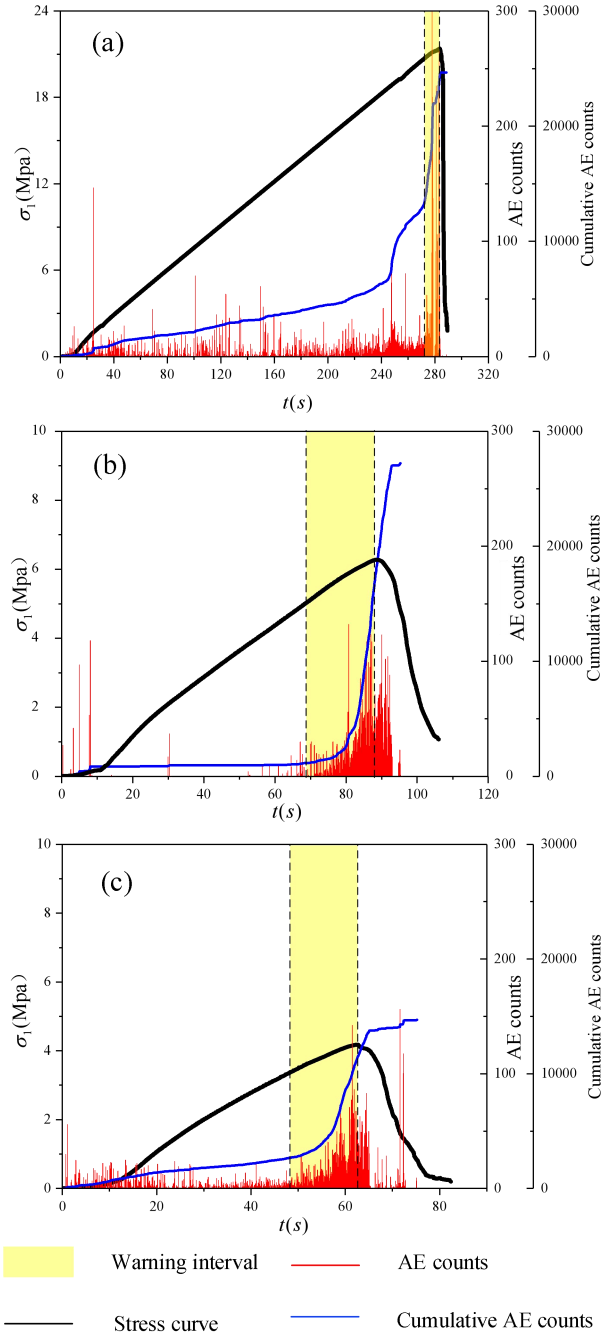

Fig. 4. Evolution of accumulative count of CPB samples with different cementing material ratio: (a)C/G=1:0 (b) C/G=3:1 (c) C/G=1:1

The samples with a cement/gypsum ratio of 1:0 presented higher AE ringing counts than those with

cement/gypsum ratios of 3:1 and 1:1 in the compaction and elastic stage, and the damage was more severe during loading. The yield phase of the stress-strain curve was relatively short, and brittle failure of the sample occurred without obvious premonition. However, in the samples that used gypsum to replace cement with equal mass, the AE ringing counts in the compaction and elastic stages were at a low level. The strength of the weak bond inside the sample was significantly lower than that of the sample with a cement/gypsum ratio of 1:0. There was an obvious transition period of AE ringing counts in yield phase, and the crack propagation before failure had an obvious omen.

It indicated that gypsum can increase the ductility of samples, making it possible to predict the occurrence of failure by picking up AE disaster signals. In engineering applications, how to set the proportion of gypsum added to make CPB samples meet both strength requirements and economic needs has become a focus of attention.

3.1.4 Effect of loading rate on AE characteristic

Fig.5 shows the CPB AE ring counting curve at different loading rates. The maximum level of AE ring count has not changed significantly and remains at about 100. With the increase of loading rate, the relative warning area becomes longer, and the peak value of AE ringing count lags obviously relative to the peak intensity. The peak value of the AE ringing count of the sample of 100N/s occurred before the peak intensity, and the peak value of the AE ringing count of the sample of 150N/s occurred from before to after the peak intensity, while the peak value of the AE ringing count of the sample of 200N/s appeared 10s after the peak intensity.

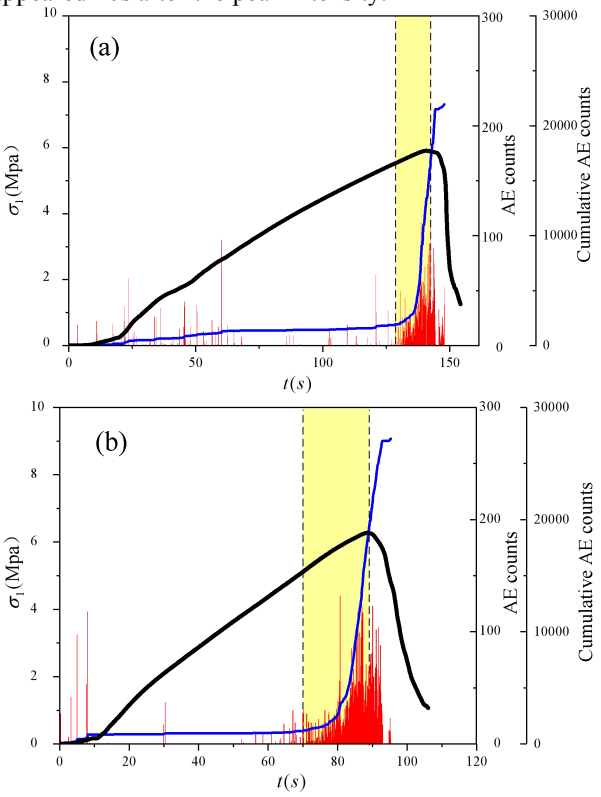

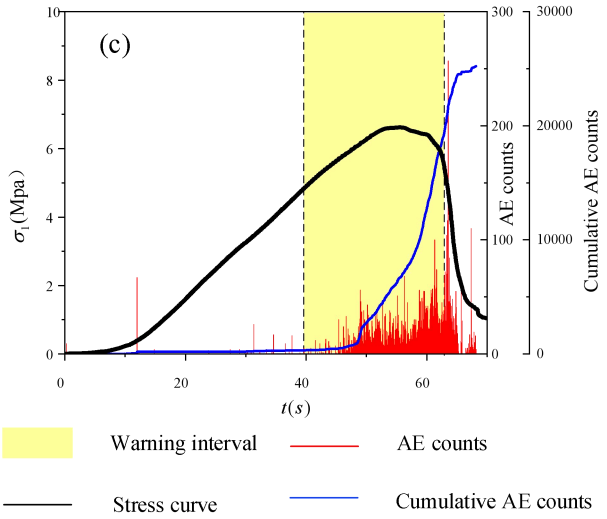

Fig. 5. Evolution of accumulative count of CPB samples with different loading rates: (a) 100N/s (b) 150N/s (c) 200N/s

The loading rate has a great influence on the AE characteristics of CPB samples, as is shown in Fig.6. In the early stage of loading, the properties of samples with different loading rates were not very different. After the yield stage, CPB samples with different loading rates showed different AE characteristics. Under the loading rate of 100N/s, yield phase of the stress-strain curve of samples was very short, and the failure mode was inclined to brittle failure. The cumulative AE ringing counts increased within a short time before reaching the peak strength, and then the ringing counts decreased rapidly. Several ringing counts peaks appeared around the failure of the samples. Yield phase of the total stress-strain curve of the sample with a loading rate of 150N/s became longer, low-level AE ringing counts frequently occurred before reaching the peak strength. The AE ringing counts without fluctuating significantly indicated that there were small cracks but no main failure surface generated inside samples. When the peak strength was reached, the peak value of AE ringing counts appeared with the main failure surface generated. For the samples with a loading rate of 200N/s, the failure mode changed from brittle failure to ductile failure. AE ringing counts appeared continuously and frequently in a long stage with multiple peaks formed. After the peak strength, the strength of the CPB sample did not decrease rapidly, some deformation still occurred under the condition of maintaining high-stress level, and a large number of AE signals could still be acquired. Subsequently, the maximum AE ringing count appeared, and the stress dropped rapidly, indicating that the sample was destroyed and lost its strength.

The concentrated generation of AE ringing counts in a certain stage can often indicate the process of a failure surface from crack propagation to crack destruction, which is represented as a peak and valley in the AE ringing count diagram. The level of the AE ringing count tended to rise, and dropped rapidly after the occurrence of a maximum, which means that a stress surface cracked and failed under the function of stress, and the stress distribution inside the sample changed.

Fig.6 shows the partially enlarged drawing of AE ringing counts and the failure surface distribution during sample failure. The sample with a loading rate of 100N/s showed splitting failure, with only one major failure surface corresponding to a peak in the AE ringing count diagram. And the rest were fine minor split cracks. The sample with a loading rate of 150N/s was characterized by both splitting failure and shear failure. There were some local shear cracks and two through cracks on the sample, one of which had the characteristics of shear failure. The characteristics of shear failure of the sample with a loading rate of 200N/s became more apparent. Except for a through-crack, a shear surface was inclined to segment the sample, and several cracks intersected the shear surface, forming several failure surfaces with local coincidence. It can be clearly seen from Fig.7(c) that the AE ringing counts of samples with a high loading rate presents multiple discontinuous dense areas with multiple peaks, which corresponds to the formation of multiple local shear cracks and major failure surfaces. Combined with the figures, it can be verified that in the sample with a loading rate of 200N/s, local failure occurred first, resulting in a local shear surface that affected the strength of the sample but did not cause complete failure of the sample. With the subsequent loading, the local shear surfaces were expanded and merged into a penetrating shear plane, and the sample was destroyed.

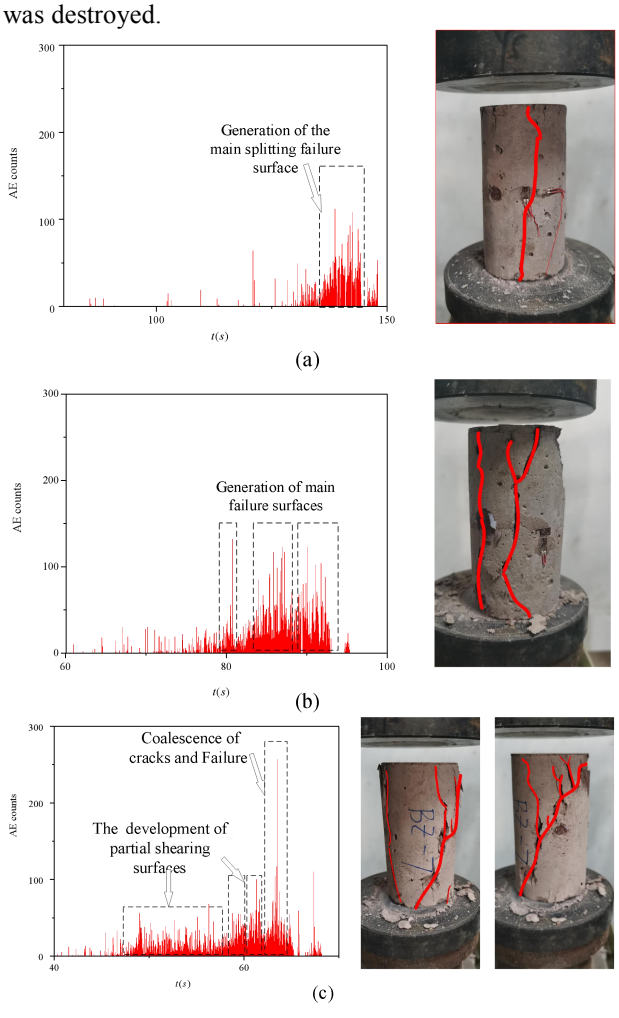

Fig. 6. Local magnified view of AE ringing count and corresponding failure surface distribution during sample failure: (a) 100N/s (b) 150N/s (c) 200N/s

3.2 Damage model based on AE ringing count

The AE signal generated during the loading process of the CPB sample can represent the expansion, connection, and coalescence of cracks inside the sample, which will cause internal damage of rock, resulting in rock deterioration and failure. Compared with AE energy and impact, AE ringing count can reflect the development of microscopic cracks better [44]. In this paper, AE ringing counts were used to represent the internal damage evolution law of CPB samples during the loading process, which can accurately warn the failure and instability of CPB through non-destructive monitoring.

The damage variable D is introduced

$$D = \frac{A_d}{A} \tag{2}$$

where A_d is the total area of micro defects in the compression section, and A is the total area of the compression surface under initial nondestructive conditions.

The AE ringing count C_w when unit area element damaged is

$$C_w = \frac{C_0}{A} \tag{3}$$

where C0 is the cumulative AE ring count when the whole section A of nondestructive material is completely destroyed.

At this point, the damage variable D when the damaged area reaches Ad can be expressed as

$$D = \frac{C_d}{C_0} \tag{4}$$

where Cd is the cumulative AE ringing count when the damaged area reaches A_d.

However, during the experiment, when the sample reached the peak strength, the sample section did not completely fail. Therefore, the damage critical value Du was introduced to modify the damage variable as

$$D = D_u \cdot \frac{C_d}{C_0} \tag{5}$$

For the sake of calculation, Du is usually evaluated as

$$D_u = 1 - \frac{\sigma_p}{\sigma_c} \tag{6}$$

where σ_p is the residual strength of the sample, and σ_c is the peak strength of the sample.

Therefore, the relationship between sample damage and time-based AE ringing count is shown in Fig.8. It can be seen from the figure that the time-damage curve has obvious characteristics of periodic changes, showing a linear - exponential - linear change trend basically. (I) In the initial stage, corresponding to the crack compaction stage in the specimen compression process, the damage value is close to 0. (II) In the stable development stage, corresponding to the elastic deformation stage, the damage shows a linear change

trend. (III) In the rapid development stage, corresponding to the failure stage of the sample, the damage value presents an exponential upward trend. (IV) In the later stage of failure, the damage value changes linearly again and gradually approaches the maximum damage value D_{max} at the corresponding strain softening and residual deformation stages.

By piecewise function analysis of time-damage curve, the fitting relationship between damage value D of CPB sample and loading time T under different conditions can be obtained as follows:

$$D = \begin{pmatrix} c_1 t + c_2, & t < t_a \\ c_3 \exp(-t / c_4) + c_5, & t_a < t < t_b \\ c_6 t + c_7, & t_b < t < t_c \end{pmatrix} \quad (7)$$

Table 3. Piecewise fitting parameters

	c_1	c_2	c_3	c_4	c_5	c_6	c_7	t_a	t_b	R^2
CPB-1	2.35E-4	0.00126	-3.87E24	1.90201	0.52684	0.05051	-5.23443	109	111.87	0.959
CPB-2.5.8	3.81E-4	0.01001	1.51E-11	-3.63176	0.03396	0.05311	-4.12946	65.48	88.09	0.995
CPB-3	0.0074	-0.0855	3.87E-6	-8.10168	0.4299	0.01408	-0.55788	77.11	89.47	0.996
CPB-4	9.36E-4	-0.0060	-2.83E7	13.092	0.4679	0.03626	-9.3766	243	270.67	0.948
CPB-6	0.0029	0.01966	0.00122	-9.64423	-0.0931	3.50E-4	0.90096	51.91	64.88	0.993
CPB-7	6.81E-4	-0.00259	0.00134	-19.6533	-1.2666	0.01256	-1.03367	135.96	144	0.995
CPB-9	7.21E-4	-0.0106	1.11E-4	-7.2733	-0.03223	0.0118	-0.02618	45	64.26	0.997

After piecewise fitting with Origin, the fitting results and parameters are shown in Table 3

When the time-damage curve reached the second stage, a large amount of AE signals began to appear and the damage value began to rise rapidly. Therefore, the damage value reaching the second stage can be judged as the precursor of peak failure of the sample, the phase from ta to tb in the curve can be regarded as a relative warning area [23].

4 Conclusion

In this paper, a uniaxial compression test was carried out on the CPB sample with a Talbot index of 0.5, and the influences of different loading rates, moisture content, and cementing material ratio on the AE characteristic of CPB were analyzed. The failure mechanism of CPB samples were discussed based on their AE characteristics. The conclusions are as follows.

(I) The ductility of CPB samples can be changed by loading rate, moisture content, and ratio of cementing materials. With the increase of loading rate, moisture content, and gypsum quality in the cementing material, the ductility of CPB increases, while the strength decreases. The corresponding AE signal is the warning area before the failure occurs, which shows that the AE ringing times gradually increase, and the cumulative AE ringing times curve begins to show an obvious upward trend. Some AE signals are generated after the peak strength.

(II) CPB sample without gypsum has higher strength and hardness, and sudden and severe damage occurs when its strength reaches a peak value. And there is no obvious tendency for the AE ringing counts to increase before failure. The addition of gypsum will reduce the strength and peak strain of the CPB sample, but it can increase the ductility of the CPB sample and significantly increase the AE ringing counts level before the failure. Therefore, CPB can be an early warning by adjustment of cement ratio, and the failure of backfill can be dealt timely with AE signal monitoring.

(III) The moisture content will change the mechanical properties and AE signal distribution of the CPB sample. With the increase of moisture content, the strength of CPB samples and the average level of AE ringing counts decrease, meanwhile, AE ringing counts are more widely distributed, and the peak value of AE ringing counts will lag. Therefore, during the filling process, the moisture content of the filling area should be controlled to ensure the strength of CPB and the timeliness of AE monitoring.

(IV) The failure mode of CPB varies with the loading rate. With the increase of loading rate, the splitting failure of single crack gradually changes to shear failure of multiple cracks

(V) The damage model based on AE indicates that the damage value of the sample presents a linear-exponential - linear change, in which the stage of exponential change is a relative warning area, which can be used as a basis for judging the impending failure of CPB in AE monitoring.

This work was funded by the National Natural Science Foundation of China (52074352).

References

1. Z. Bian, X. Miao, S. Lei, et al. The Challenges of Reusing Mining and Mineral-Processing Wastes. Science, **337(6095)** 702-703, (2012)
2. X.X. Miao, J.X. Zhang, M.M. Feng. Waste-filling in fully-mechanized coal mining and its application. Journal of China University of Mining and Technology, **18(4)** 479-482, (2008)
3. S. Cao, W. Song. Effect of filling area time on the mechanical strength and ultrasonic properties of

cemented coarse tailing backfill. International Journal of Mineral Processing, **166**(62-68), (2017)

4. Z. Lu, M. Cai. Disposal Methods on Solid Wastes from Mines in Transition from Open-Pit to Underground Mining. Procedia Environmental Sciences, **16**(715-721), (2012)
5. D.R. Tesarik, J B Seymour, T R Yanske. Long-term stability of a backfilled room-and-pillar test section at the Buick Mine, Missouri, USA. International Journal of Rock Mechanics and Mining Sciences, **46(7)**: 1182-1196, (2009)
6. M.L. Bloss. An operational perspective of mine backfill//Y Potvin, T Grice. Eleventh International Symposium on Mining with Backfill. Perth; Australian Centre for Geomechanics. 15-30 (2014)
7. V.I. Cheskidov, A.V. Reznik. Features of Hydraulic Fill Formation in Mining Water-Bearing Lignite Deposit. Journal of Mining Science, **55(2)**: 273-279, (2019)
8. W.Y. Lv, Z.H. Zhang. Research on the Belt Loader Waste Rock Gravity Backfill Mining Technology. Applied Mechanics and Materials, **253-255**(253-255), (2012)
9. X. Li, J. Du, L. Gao, et al. Immobilization of phosphogypsum for cemented paste backfill and its environmental effect. Journal of Cleaner Production, **156**(137-146), (2017)
10. L. Chen, X. Xu, J. Wu, et al. Characteristics Variation of Tailings Using Cemented Paste Backfill Technique. Water, Air, & Soil Pollution, **225(5)**: 1974, (2014)
11. P. Jongpradist, S. Youwai, C. Jaturapitakkul. Effective Void Ratio for Assessing the Mechanical Properties of Cement-Clay Admixtures at High Water Content. Journal of Geotechnical and Geoenvironmental Engineering, **137(6)**: 621-627, (2011)
12. J. Wu, M. Feng, G. Han, et al. Experimental Investigation on Mechanical Properties of Cemented Paste Backfill under Different Gradations of Aggregate Particles and Types and Contents of Cementing Materials. Advances in Materials Science and Engineering, **2019**: 11, (2019)
13. Z.X. Liu, X.B, Li. Study on Fractal Gradation of Tailings and Knowledge Bank of Its Cementing Strength. Chinese Journal of Rock Mechanics and Engineering, **(10)**: 1789-1793, (2005)
14. J. Wu, M. Feng, Z. Chen, et al. Particle Size Distribution Effects on the Strength Characteristic of Cemented Paste Backfill. Minerals, **8(8)**: 322, (2018)
15. E. Yilmaz. Sustainability and Tailings Management in The Mining Industry: Paste Technology. Mugla Journal of Science and Technology, **1**: (2018)
16. X. Zhang, G. Ruiz, A.M. Elazim. Loading rate effect on crack velocities in steel fiber-reinforced concrete. International Journal of Impact Engineering, **76** 60-66, (2015)
17. A.L. Rosa, R.C. Yu, G. Ruiz, et al. A loading rate dependent cohesive model for concrete fracture. Engineering Fracture Mechanics **82** 195-208, (2012).
18. X.Q. Fan, S.W. Hu, J. Lu, et al. AE properties of concrete on dynamic tensile test. Construction and Building Materials, **114** 66-75, (2016).
19. J.W. Archer, M.R. Dobbs, A. Aydin, et al. Measurement and correlation of AEs and pressure stimulated voltages in rock using an electric potential sensor. International Journal of Rock Mechanics and Mining Sciences, **89** 26-33, (2016).
20. X. Yang, X.R. Liu, K. Zhao, et al. Application of AE time series in the study of the damage process of tailing cemented backfill under uniaxial compression. Electronic Journal of Geotechnical Engineering, **18** I 1739-1756, (2013)
21. X. Liu, K. Liu, K. Zhao, et al. Strain rate effects and AE characteristics of tailing cement backfill under uniaxial compression. Electronic Journal of Geotechnical Engineering, **18** R 3919-3932, (2013)
22. A.Y. Cao, G.C. Guang, L.M. Dou, et al. Damage evolution law based on AE of sandy mudstone under different uniaxial loading rate. Journal of Mining & Safety Engineering, **32(06)**: 923-928+35, (2015)
23. J.X. Ren, S. Jing, C.K. Liu. Experimental Study on Deformation and Failure Laws and AE Characteristics of Weak Cemented Sandstone. Coal Technology, **38(06)**: 1-4, (2019)